

1 **Title**

2 A 3D individual-based model to investigate the spatially heterogeneous response of bacterial
3 biofilms to antimicrobial agents

4 Lakshmi Machineni, Ch. Tejesh Reddy, Vandana Nandamuri, Parag D. Pawar
5 Department of Chemical Engineering, Indian Institute of Technology Hyderabad, India
6

7

8

9

10

11

12

13

14

15

16

17

18

19

20

21

22

23 Corresponding Author

24 Parag D. Pawar

25 Department of Chemical Engineering

26 Indian Institute of Technology Hyderabad

27 Kandi, Sangareddy – 502285

28 Telangana 502 205, India

29 Tel.: +91 40 2301 6068

30 Fax: +91 40 2301 6032

31 Email: parag@iith.ac.in

32

33

34 Keywords: biofilms; antibiotic resistance; cellular automata; heterogeneity;

35

36 **Abstract**

37

38 The response of bacterial biofilms to treatment with antimicrobial agents is often characterized
39 by the emergence of recalcitrant cellular microcolonies. We present an individual-based model
40 to investigate the biophysical mechanisms of the selective resistance that arises within the
41 biofilm and leads to a spatially heterogeneous response upon treatment with antibiotics. The
42 response occurs in three distinct phases. In the first phase, the subpopulation of metabolically
43 active cells diminishes due to antibiotic-induced cell death. Subsequently, in the second phase,
44 increased nutrient availability allows dormant cells in the lower layers of the biofilm to transform
45 into metabolically active cells. In the third phase, survival of the biofilm is governed by the
46 interplay between two contrasting factors: (i) rate of antibiotic-induced cell death, and (ii) rate of
47 transformation of dormant cells into active ones. Metabolically active cells at the distal edge of
48 the biofilm sacrifice themselves to protect the dormant cells in the interior by (i) reducing local
49 antibiotic concentrations, and (ii) increasing nutrient availability. In the presence of quorum
50 sensing, biofilms exhibit increased tolerance compared to the quorum sensing-negative strains.
51 EPS forms a protective layer at the top of the biofilm, thereby limiting antibiotic penetration.
52 The surviving cells, in turn, produce EPS resulting in a feedback-like mechanism of resistance.
53 Whereas resistance in QS^- biofilms occurs because of transformation of dormant cells into
54 metabolically active cells, this transformation is less pronounced in QS^+ biofilms, and resistance
55 is a consequence of the sequestration of the antibiotic by EPS.

56

57

58 **Introduction**

59 Biofilms are surface-associated communities of microorganisms embedded in an extracellular
60 matrix composed primarily of self-produced polysaccharides [1, 2]. Biofilms shelter bacteria
61 from environmental stresses and from the host immune response, thereby increasing resistance to
62 antibiotics and phagocytosis, as well as to other components of the innate and adaptive immune
63 systems [3, 4]. Several mechanisms -- acting synergistically -- contribute to the reduced
64 antimicrobial and biocide susceptibility that is characteristic of biofilm communities. Expression
65 of specific genes may allow biofilm bacteria to actively adapt to, and survive, antimicrobial
66 exposure [5-9]. For instance, the *ndvB* locus has been identified as a *Pseudomonas aeruginosa*
67 (*P. aeruginosa*) biofilm-specific antibiotic resistant gene; *ndvB* biofilms were 16-fold more
68 susceptible to tobramycin and 8-fold more susceptible to both gentamicin and ciprofloxacin than
69 wild-type biofilms [10]. In response to antibiotic treatment, overexpression of toxins that inhibit
70 essential functions such as translation may contribute to the transformation of biofilm bacteria to
71 an antibiotic tolerant phenotype [11]. These genetic mechanisms attribute resistance of the
72 biofilm to antibiotic tolerance at the single-cell level [12, 13].

73 Antibiotic resistance may also emerge as a consequence of physiological characteristics inherent
74 to the biofilm mode of growth [1, 14]. Biofilms are characterized, among other things, by the
75 presence of nutrient and antibiotic gradients, diffusion and penetration limitations, and a matrix
76 of extracellular polymeric substances (EPS) [15-17]. Bacteria growing in biofilms are
77 physiologically heterogeneous, due in part to their adaptation to local environmental conditions.
78 They occupy a spectrum of growth states from rapidly growing and active to slow-growing and
79 dormant. Consequently, distinct microcolonies with clusters of bacterial cells may develop
80 within the biofilm where cellular physiology is different from surroundings in terms of metabolic
81 activity, secretion of EPS, and concentrations of nutrients and antimicrobial agents [17-20]. This
82 intrinsic physiological heterogeneity of biofilms may play a role in the adaptive stress response,
83 and contribute to the protection of cells [21]. Experimental evidence suggests that it is only
84 certain subpopulations within biofilms that show greatly increased phenotypic resistance to
85 treatment, whereas the remaining cells exhibit sensitivity [22-24]. A particular antimicrobial
86 agent may effectively target certain populations of cells, but leave the remaining cells viable,
87 allowing them to repopulate the biofilms when the treatment is stopped. For instance, cells deep
88 within *P. aeruginosa* biofilms are reported to be in a metabolically inactive, antibiotic-tolerant
89 state, whereas cells at the periphery are faster growing, and susceptible to antimicrobial agents
90 such as ciprofloxacin, tetracycline, and tobramycin [25, 26]. The biophysical mechanisms
91 underlying this spatially non-uniform response of biofilms to antimicrobial treatment remain
92 incompletely understood.

93 The lowest concentration of the antimicrobial agent required to eradicate the biofilm is termed
94 the minimum biofilm eradication concentration (MBEC) [27]. Subjecting the biofilm to sub-
95 lethal concentrations of the antibiotic (sub-MBEC) enhances biofilm formation *in vitro* [28-30].
96 For instance, subjecting *P. aeruginosa* biofilms to sub-MBEC treatment induces genetic triggers
97 that result in the enhanced formation of colonic acid [31]. This, in turn, causes an increase in the
98 synthesis of EPS which contributes to the protection of the bacterial population. Antibiotic-
99 induced biofilm formation has clinical relevance because bacteria are exposed to low
100 concentrations of antibiotics at the beginning and the end of treatment, or continuously during
101 low-dose therapy [30]. Investigating the reasons for survival of biofilms in response to sub-

102 MBEC treatment of antibiotics may help delineate biophysical mechanisms of antibiotic
103 resistance.

104 Quorum sensing (QS) is a process by which bacteria coordinate their behavior in a cell-density
105 dependent manner by producing and detecting signaling molecules called autoinducers [32-34].
106 QS has been shown to control the amount of EPS synthesis in *P. aeruginosa* biofilms [35-39].
107 Furthermore, experimental investigations support the role of QS-regulated EPS in the resistance
108 of *P. aeruginosa* biofilms to antibiotic treatment [40]. The EPS matrix protects the biofilm by
109 impeding penetration of tobramycin via ionic interactions at the periphery [39, 41]. In addition,
110 antibiotic susceptibility of *Staphylococcus aureus* biofilms towards vancomycin increases in the
111 presence of QS-inhibitors by deactivating EPS biosynthesis [42]. Nutrient concentration
112 gradients in QS⁺ biofilms may induce spatio-temporal heterogeneity in autoinducer secretion,
113 which may, in turn, result in microscale variation in EPS production. How the spatial
114 heterogeneity of EPS influences the heterogeneous response of biofilms to antibiotics is currently
115 not known.

116 We have previously formulated and analyzed a three-dimensional, individual-based
117 computational model to simulate biofilm growth dynamics, and to quantify spatial heterogeneity
118 in the bacterial population as a function of nutrient availability and quorum sensing [43]. The
119 model treats bacterial cells as individual entities with their own states, thereby allowing for
120 variability between individual behaviors with respect to their growth rates, antibiotic and nutrient
121 uptake rates, autoinducer production, up-regulation and down-regulation states, and EPS
122 secretion. The individual-based, discrete nature of the model, combined with physical dynamics
123 causes chemical and structural heterogeneities within the biofilm to emerge as a consequence of
124 the actions and interactions of the cells with each other, and with the surrounding environment,
125 rather than being a model input. In this work, we investigate the response of QS⁻ and QS⁺
126 biofilms to treatment with antibiotics, and the influence of heterogeneity on this response. The
127 goal was to answer the following questions: (1) Do local physiological and chemical
128 heterogeneities in the biofilm influence the spatially heterogeneous antibiotic resistance in the
129 absence of genetic triggers? (2) What roles do biophysical and cellular processes play in
130 enhanced biofilm formation in response to treatment with sub-lethal doses of antibiotics? (3)
131 What role does EPS play in the heterogeneous response of the biofilm to antibiotic treatment?
132 Our results indicate that during the initial stages of treatment, the proportion of the fast-growing,
133 metabolically active subpopulation decreases due to exposure to the antibiotic. This results in an
134 increase in the nutrient availability to the dormant cells in the inner regions of the biofilm. We
135 propose that this triggers a transformation from the dormant state to the metabolically active
136 state, and that this transformation is a key mechanism of resistance. When subjected to sub-
137 MBEC treatment, antibiotic-induced cell death at the biofilm surface leads to increased nutrient
138 availability in the inner regions, resulting in enhanced growth compared to the untreated biofilm.
139 Due to the protective influence of EPS, QS⁺ biofilms required a higher concentration of the
140 antibiotic to eradicate compared to the QS⁻ biofilms.

141

142

143 **Methods**

144

145 *Model description and simulation domain*

146 We used a 3D individual-based model to simulate the growth dynamics of a bacterial biofilm in
147 response to treatment with antibiotics. Biofilm growth is simulated within a rectangular box
148 whose bottom surface (120 μm x 120 μm) represents the inert substratum. A reservoir of
149 nutrient is placed at the top at a constant distance from the substratum, and is continuously
150 replenished so that a constant concentration is maintained in the bulk phase. The interface
151 between the reservoir and the biofilm domain is termed the diffusion boundary layer (DBL). The
152 space between the DBL and the substratum is discretized into cubical elements of volume 27
153 μm^3 each. During the simulation, each element may be occupied by one or more of the
154 following entities: (i) bacterial cell, (ii) EPS, (iii) nutrient, (iv) autoinducer, and (v) antibiotic.
155 Periodic boundary conditions are applied in the horizontal directions, thereby eliminating edge
156 effects, and ensuring continuity of biomass [44, 45]. Each bacterium is modeled as a distinct
157 entity with its own set of parameter values and behaviors. To simulate behavioral variability,
158 parameter values for individual bacterial cells are obtained by random draws from a uniform
159 distribution around the values listed in Table 1. The simulation represents a time march in which
160 the occupancy state of each element is updated at every time step. At time $t = 0$, six cells, termed
161 colonizers, are placed into random elements atop the substratum. Simultaneously, nutrient
162 diffuses across the DBL. Cells consume nutrient, and subsequently grow and divide, resulting in
163 the formation of a contiguous multicellular population. At the end of each time step, the nutrient
164 reservoir is shifted vertically upwards such that a pre-determined distance from the topmost cell
165 in the biofilm is always maintained.

166

167 *Assumptions*

168 The following are the key assumptions made:

- 169 (1) The biofilm does not pose an obstacle to flow, and is subjected to a constant linear velocity
170 gradient of 10 s^{-1} with zero velocity at the substratum, and maximum velocity at the highest
171 point. It has been shown that giving up the conservation principles for fluid flow in the
172 biofilm domain leads to increased deviations with respect to concentration fields and fluxes
173 [46]. The magnitude of deviation is in some cases small ($< 2\%$, at slow bulk flow velocities
174 of $\sim 0.0001 \text{ ms}^{-1}$), and considerable in other ($> 20\%$, at fast bulk flow velocities of 0.01 ms^{-1}).
175 The results presented in this work correspond to the low bulk flow regime (maximum
176 velocity of $\sim 0.0006 \text{ ms}^{-1}$). Consequently, deviations in concentration fields and fluxes have
177 been neglected. Such low fluid shear rates ($10\text{-}50 \text{ s}^{-1}$), experienced within the intestine, and
178 veins, have been shown to be effective in simulating *S. aureus* biofilm colonization and
179 development [47, 48].
- 180 (2) The DBL remains parallel to the substratum throughout the simulation. It is worth noting
181 that at high fluid velocities, the diffusion boundary could follow the surface of the biofilm,
182 and may not be necessarily stratified as is assumed here [49].
- 183 (3) The DBL has a constant thickness of 18 μm . For the low-flow regime considered in this
184 work, the nutrient concentration at a vertical distance of 18 μm from the highest cell in the

185 biofilm was greater than 95% of the bulk nutrient concentration, even at time points
 186 corresponding to the highest cell numbers.

187 (4) EPS is capable of coexisting with a bacterial cell within a cubical element. This is consistent
 188 with previous experimental work showing the accumulation of extracellular polysaccharides
 189 such as β -glucan found intercalating between micro colonies of *Streptococcus mutans* [50].
 190 Consequently, we assume that new bacterial cells embed themselves into existing EPS,
 191 instead of pushing it aside.

192 (5) Negative parameter values of individual bacterial cells, or those outside $\pm 10\%$ of the mean
 193 were discarded; these precautions are necessary with distributions ranging from $-\infty$ to $+\infty$.

194

195 A full mathematical description of the various components and processes incorporated in the
 196 model has been presented elsewhere [43]. Here, we briefly present the governing equations,
 197 behaviors of the particulate and soluble entities, and the numerical scheme used.

198

199 *Nutrient reaction and transport*

200 The rate of consumption of the nutrient by bacteria is a function of the concentrations of the
 201 biomass ($C_B(\bar{x}, t)$) and the nutrient $C_N(\bar{x}, t)$ at the spatial coordinates \bar{x} and time t , and is given
 202 by

203

$$204 \quad r_N(\bar{x}, t) = \left(\frac{\mu_{max}}{Y_{NB}} + m \right) C_B \left(\frac{C_N(\bar{x}, t)}{C_N(\bar{x}, t) + K_N} \right) \quad (1)$$

205

206 where μ_{max} is the maximum specific growth rate, Y_{NB} and m are the yield and maintenance
 207 coefficients, respectively, and K_N is the half saturation concentration of the nutrient (N). The
 208 nutrient concentration field is governed by the reaction-diffusion-convection equation (Eq. 2)

209

$$210 \quad \frac{\partial C_N(\bar{x}, t)}{\partial t} = -r_N(C_N(\bar{x}, t), C_B(\bar{x}, t)) + D_N \sum_{i=1}^3 \frac{\partial^2 C_N(\bar{x}, t)}{\partial x_i^2} - \nabla \cdot (v C_N) \quad (2)$$

211

212 Here, D_N is the nutrient diffusivity, and v is the local fluid velocity. $C_N(\bar{x}, t)$ is set to $C_{N,bulk}$
 213 at the top surface, and to 0 at the substratum. Periodic boundary conditions are applied at the
 214 lateral boundaries.

215

216 *Biomass growth*

217 Consumption of nutrient leads to cell growth, and endogenous metabolism. Endogenous
 218 metabolism is assumed to be proportional to the biomass concentration. The leftover nutrient is
 219 utilized for cell growth at an efficiency Y_{NB} . The net accumulation of biomass is, given by:

220

$$221 \quad \frac{\partial C_B(\bar{x}, t)}{\partial t} = Y_{NB} [r_N(C_N(\bar{x}, t), C_B(\bar{x}, t)) - m C_B(\bar{x}, t)] \quad (3)$$

222

223

224 *Cell division*

225 When the biomass of a cell increases to twice its native value it divides into two daughter cells.
226 One daughter cell continues to occupy the same element as the mother cell, while the other is
227 pushed into a cell-free element in the immediate, Moore neighborhood. For each cell, the Moore
228 neighborhood, comprises of 26 cubical elements surrounding the central element. If multiple
229 cell-free elements are available for occupation, one is chosen at random. On the other hand, if all
230 elements in the Moore neighborhood are occupied by bacteria, an unoccupied element is
231 identified at the nearest Chebyshev distance from the location of the mother cell. The occupancy
232 statuses of elements are checked at successively larger Chebyshev distances (starting with a
233 Chebyshev distance of 2, and moving outward, layer by layer), until an empty element is found.
234 Each of the cells that lies between the mother cell and the closest cell-free element is then shifted
235 by one grid element – away from the mother cell, and towards the empty element – creating a
236 cell-free element in the Moore neighborhood of the mother cell. This newly created cell-free
237 element is then occupied by the daughter cell, thereby ensuring that the daughter cell is always
238 placed immediately next to the dividing bacterium [43].

239

240 *Cell death*

241 The nutrient uptake rate (R) is defined as the ratio of the nutrient uptake rate (r_N) to endogenous
242 metabolism (mC_B). There are three mechanisms by which a bacterium can die: (i) limited
243 nutrient uptake rate (R), (ii) stay in the stationary phase for a predetermined number of hours
244 (t_{SP}), and (iii) exposure to antibiotic. If $R > 1$, the bacterium exhibits net growth. On the other
245 hand, for $R < 1$, the bacterium shows negative net growth, and is said to have entered the
246 stationary phase. Bacteria die if R falls below a certain threshold (R_{min}). This is an attempt to
247 account for bacterial death under nutrient starvation conditions. Bacteria also die if they have
248 been in this growth-arrested phase for a pre-specified number of hours (t_{SP}). This is recorded
249 with an individual based counter. If R is below 1 during one hour, the counter increases by one.
250 However, a bacterium also has the possibility to recover if R increases above 1 before it dies.
251 Consequently, if R is above 1 during one hour, the counter decreases by one. The counter can
252 never be less than zero. Moreover, if the biofilm is subjected to antibiotic treatment, then cells
253 die based on probability of killing by antibiotic which is a function of the rate of consumption of
254 antibiotic (Eq. 13).

255

256 *Cell detachment*

257 We implement a simplified geometrical model of cell detachment governed by (i) localized cell
258 death, and (ii) EPS formed as a consequence of quorum sensing. Cell detachment is determined
259 by evaluating the connectivity of cells to the substratum. Within the biofilm, bacteria connect to
260 the substratum either directly, or indirectly through a group of live bacteria in which at least one
261 bacterium is directly bound to the substratum [51]. In addition to live bacteria, in QS^+ biofilms,
262 cells can also continue to remain connected to the substratum via EPS. At the end of each time
263 step, detachment events are recorded, and detached cells are removed from the domain.

264

265

266 *Quorum Sensing*

267 Every bacterium that engages in quorum sensing is allowed to switch randomly between the up-
 268 regulated, and the down-regulated state, at rates, dependent on the local autoinducer
 269 concentration ($C_A(\bar{x}, t)$) in the grid element. At time $t = 0$, all the bacteria are in the down-
 270 regulated state. The transition rate from the down-regulated to up-regulated state is given by

$$TR^+ = \alpha \frac{C_A(\bar{x}, t)}{1 + \gamma C_A(\bar{x}, t)} \quad (4)$$

271
 272 While, the transition rate between the up-regulated to down-regulated states is given by [52]

$$TR^- = \beta \frac{1}{1 + \gamma C_A(\bar{x}, t)} \quad (5)$$

273 where α and β are the spontaneous up- and down-regulation rates, and γ is the transition
 274 constant.
 275

276
 277 Within a time interval of Δt , the probabilities of switching from one state to another are then
 278 given by

$$\begin{aligned} P_u &= (TR^+) \Delta t \\ P_d &= (TR^-) \Delta t \end{aligned} \quad (6)$$

281 where P_u is the probability of up-regulation, and P_d is the probability of down-regulation.

282
 283 For each bacterium, at every time step, the simulation generates a random number (n_R) from a
 284 uniform distribution on the interval $[0, 1]$. If $P_u > n_R$, then the bacterium switches from the
 285 down-regulated state to an up-regulated state. On the other hand, if $P_d > n_R$, then the bacterium
 286 switches from the up-regulated to the down-regulated state.

287
 288 *Autoinducer Production and Transport*

289 Up-regulated and down-regulated cells secrete autoinducer molecules at constant rates of $r_{A,u}$
 290 and $r_{A,d}$, respectively.

$$r_A = \begin{cases} r_{A,u} \\ r_{A,d} \end{cases} \quad (7)$$

291 where $r_{A,u} > r_{A,d}$ (Table I). The secreted autoinducer is treated as a dissolved entity that is
 292 transported via diffusion and convection. The time evolution of autoinducer concentration
 293 within the biofilm is given by

$$\frac{\partial C_A(\bar{x}, t)}{\partial t} = D_A \sum_{i=1}^3 \frac{\partial^2 C_A(\bar{x}, t)}{\partial x_i^2} + \frac{r_A}{\Delta V} - \nabla \cdot (v C_A) \quad (8)$$

294 where D_A is the autoinducer diffusivity, and ΔV is the element volume. Eq. 8 is subject to the
 295 Dirichlet boundary condition at the DBL ($C_{A,DBL} = 0$), and the no-flux condition at the
 296 substratum. Upregulated cells secrete autoinducer molecules and EPS at an enhanced rate,
 297 compared to their downregulated counterparts [52, 53]. In a feedback-like mechanism, enhanced

298 production of autoinducer by upregulated cells results in the upregulation of an increasing
 299 number of cells in the neighborhood.

300
 301 *EPS Production*

302 EPS is treated as a discrete entity and is tracked individually in a manner similar to that of
 303 bacterial cells. Bacterial growth and EPS production are assumed to occur concurrently from
 304 nutrient that is leftover after maintenance has been accounted for. EPS is produced only by
 305 upregulated cells, at a rate given by

$$\frac{\partial C_E(\bar{x}, t)}{\partial t} = Y_{NE} [r_N(C_N(\bar{x}, t), C_B(\bar{x}, t)) - mC_B(\bar{x}, t)] \quad (9)$$

307
 308 where, Y_{NE} is the yield coefficient for EPS, i.e. the efficiency with which unutilized nutrient is
 309 converted to EPS. EPS do not grow, die or consume nutrient, but they occupy space and
 310 undergo division. EPS division is handled similar to cell division described above, wherein
 311 daughter “EPS cells” are placed into the nearest element that does not contain EPS. The
 312 consumption of antibiotic by EPS is governed by Monod-like kinetics (Eq. 11). This is an
 313 attempt to account for the reaction-diffusion barrier to penetration by the antibiotic that EPS
 314 provides.

315
 316 *Diffusion and reaction of antibiotics*

317 In select runs, the biofilm is subjected to a continuous antibiotic treatment for a duration of 24 h.
 318 The antibiotic concentration in the bulk fluid is held constant throughout the treatment period.
 319 As the antibiotic diffuses through the DBL, live bacterial cells and EPS consume the antibiotic in
 320 a Monod-like reaction [54]. The consumption of antibiotic by non-quorum sensing bacteria is
 321 assumed to be a function of the local antibiotic concentration and biomass concentrations, is
 322 given by Eq. (10)

$$r_{ab}(C_{ab}(\bar{x}, t), C_B(\bar{x}, t)) = \left(\frac{C_{ab}(\bar{x}, t)}{C_{ab}(\bar{x}, t) + K_{ab}} \right) K_{BMax} C_B(\bar{x}, t) \quad (10)$$

323
 324 where K_{BMax} is the maximum specific reaction rate of antibiotic with respect to biomass, K_{ab} is
 325 the Monod half-saturation coefficient of antibiotic, and $C_{ab}(\bar{x}, t) = C_{ab}(x, y, z, t)$ represents local
 326 antibiotic concentration in each grid element, at time point t. In QS^+ biofilms, the consumption
 327 of antibiotic by bacteria and EPS, is given by Eq. (11).

$$r_{ab}(C_{ab}(\bar{x}, t), C_B(\bar{x}, t)) = \left(\frac{C_{ab}(\bar{x}, t)}{C_{ab}(\bar{x}, t) + K_{ab}} \right) [K_{BMax} C_B(\bar{x}, t) + K_{EMax} C_E(\bar{x}, t)] \quad (11)$$

331
 332 where K_{EMax} represents the maximum specific reaction rate of antibiotic by EPS, and C_E
 333 represents the EPS biomass. The dynamics of the antibiotic concentration field $C_{ab}(\bar{x}, t)$ is
 334 given by the following reaction-diffusion equation:
 335

336

337
$$\frac{\partial c_{ab}(\bar{x}, t)}{\partial t} = -r_{ab}(c_{ab}(\bar{x}, t), c_B(\bar{x}, t)) + D_{ab} \sum_{i=1}^3 \frac{\partial^2 c_{ab}(\bar{x}, t)}{\partial x_i^2} - \nabla \cdot (v c_{ab}) \quad (12)$$

338

339 where D_{ab} is the antibiotic diffusivity, and v is the local fluid velocity.

340

341 The probability of cell death due to antibiotic consumption is given by:

$$P_{death} = \left(\frac{r_{ab}(\bar{x}, t) - r_{Min}}{r_{Max} - r_{Min}} \right) \quad (13)$$

342

343 r_{Min} and r_{Max} are the rates of consumption of the antibiotic at minimum and maximum
 344 inhibitory concentrations of one bacterium, respectively. At each time step during treatment, a
 345 random number (n_R) is generated for each cell. If $P_{death} > n_R$, then the bacterium dies, and is
 346 removed from the simulation domain.

347

348 *Bacterial heterogeneity based on growth rates*

349 Cells within the biofilm are classified into three groups based on their growth rates: cells
 350 exhibiting (i) high (HGR), (ii) intermediate, and (iii) low growth rates (LGR). The growth rate
 351 of each cell is evaluated as the change in biomass over a period of 4 h. Growth rates vary from
 352 ~ 10 to $\sim 10,000 \text{ gm}^{-3}\text{h}^{-1}$. After 64 h of growth (in the absence of antibiotic treatment), cells are
 353 sorted from highest to the lowest growth rates. The top 10% of the cell population is classified
 354 as HGR, and the bottom 10% as LGR. This percentage of HGR is in agreement with
 355 experimental observations that suggest that the proportion of active bacteria in biofilms is range
 356 from ~ 5 -35% [55, 56]. Using this methodology, the threshold growth rate above which cells are
 357 classified as HGR is set to $6000 \text{ gm}^{-3}\text{h}^{-1}$, and that below which cells are classified as LGR is set
 358 to $425 \text{ gm}^{-3}\text{h}^{-1}$.

359

360 *Model Simulation and Numerical Scheme*

361 The simulation represents a time march in which the occupancy states of each grid element is
 362 updated at discrete time steps of 1 h. Previous work analyzing the kinetics of the switching
 363 process from the vegetative state to the competent (EPS producing) state of *Bacillus subtilis* (*B.*
 364 *subtilis*) has shown that the duration of the switching period was $1.4 \pm 0.3 \text{ h}$ [57]. In addition,
 365 analysis of *B. subtilis* at the interface between the culture medium and air indicates that bacteria
 366 switch from the motile to the matrix-producing phenotype (downregulated to upregulated)
 367 between 10 min to 1h [58]. We use a multiscale integration approach with two distinct time
 368 scales: (i) cellular processes (biomass growth (Eq. 3), EPS production (Eq. 9), switching between
 369 up- and down-regulated states (Eq. 6), death by antibiotic (Eq. 13), cell division, and
 370 detachment) are monitored every 1 h, and (ii) within this “outer” time loop, concentrations of
 371 dissolved entities (nutrient (Eq. 2), autoinducer (Eq. 8), and antibiotic (Eq. 12)) are tracked by
 372 solving the diffusion-convection equations at a finer time resolution of $1 \times 10^{-6} \text{ h}$. Numerical
 373 solutions to the diffusion-convection equations are obtained using a second-order Forward-Time
 374 Central-Space scheme. Periodic boundary conditions are applied in the horizontal directions,
 375 and the Dirichlet boundary condition is imposed in the vertical direction. The Java programming

376 language is used since it provides a convenient object-oriented framework that is well-suited for
377 the individual based model described here.

378

379 The parameter values used in the model are summarized in Table I.

380

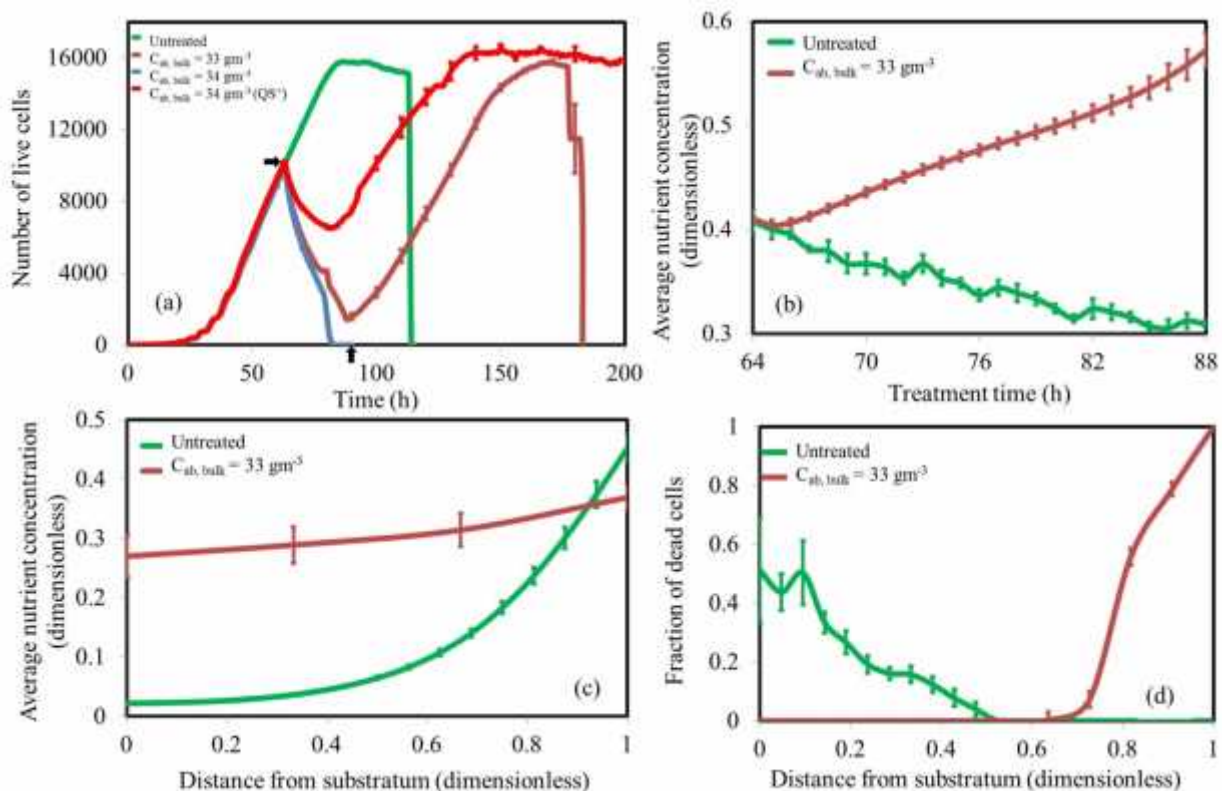
381

382 **Results**

383

384 *Biofilm growth dynamics in response to antibiotic treatment*

385



386

387

388

389 **Fig. 1. Growth dynamics of QS⁻ and QS⁺ biofilms in the absence and presence of antibiotic**

390 **treatment.** The number of live cells as a function of time for $C_{N,bulk} = 4 \text{ gm}^{-3}$ for the

391 untreated QS⁻ biofilm (green), and when subjected to a continuous 24h (64-88 h) treatment of

392 sub-MBEC ($C_{ab,bulk} = 33 \text{ gm}^{-3}$, red), and MBEC ($C_{ab,bulk} = 34 \text{ gm}^{-3}$, blue); the QS⁺ biofilm

393 is subjected to $C_{ab,bulk} = 34 \text{ gm}^{-3}$ (orange) (a), comparisons of average nutrient concentration

394 (b), spatial distribution of average nutrient concentration (c) and spatial distribution of fraction of

395 dead cells (d) for the QS⁻ biofilm subjected to sub-MBEC and the untreated biofilm. Data in

396 panels (c) and (d) are reported at 88 h, the time point at which treatment stops. The arrows in

397 panel (a) represent – initial (64 h) and end (84 h) time points of antibiotic treatment. Data

398 represent mean \pm standard error of mean (SEM) of four replicate simulations.

399

400 We simulated the growth dynamics of a bacterial biofilm over a period of 200 h, in the presence

401 and absence of QS. In select runs, the biofilm was subjected to a continuous antimicrobial

402 treatment ($C_{ab,bulk}$ ranging from 15 to 60 gm^{-3}) for duration of 24 h, initiated after 64 h of

403 growth (cell number $\sim 10,000$). Whereas subjecting the biofilm to $C_{ab,bulk}$ of 34 gm^{-3} resulted in

404 complete removal after 21 ± 0.5 h of treatment (Fig. 1a), a slightly lower antibiotic

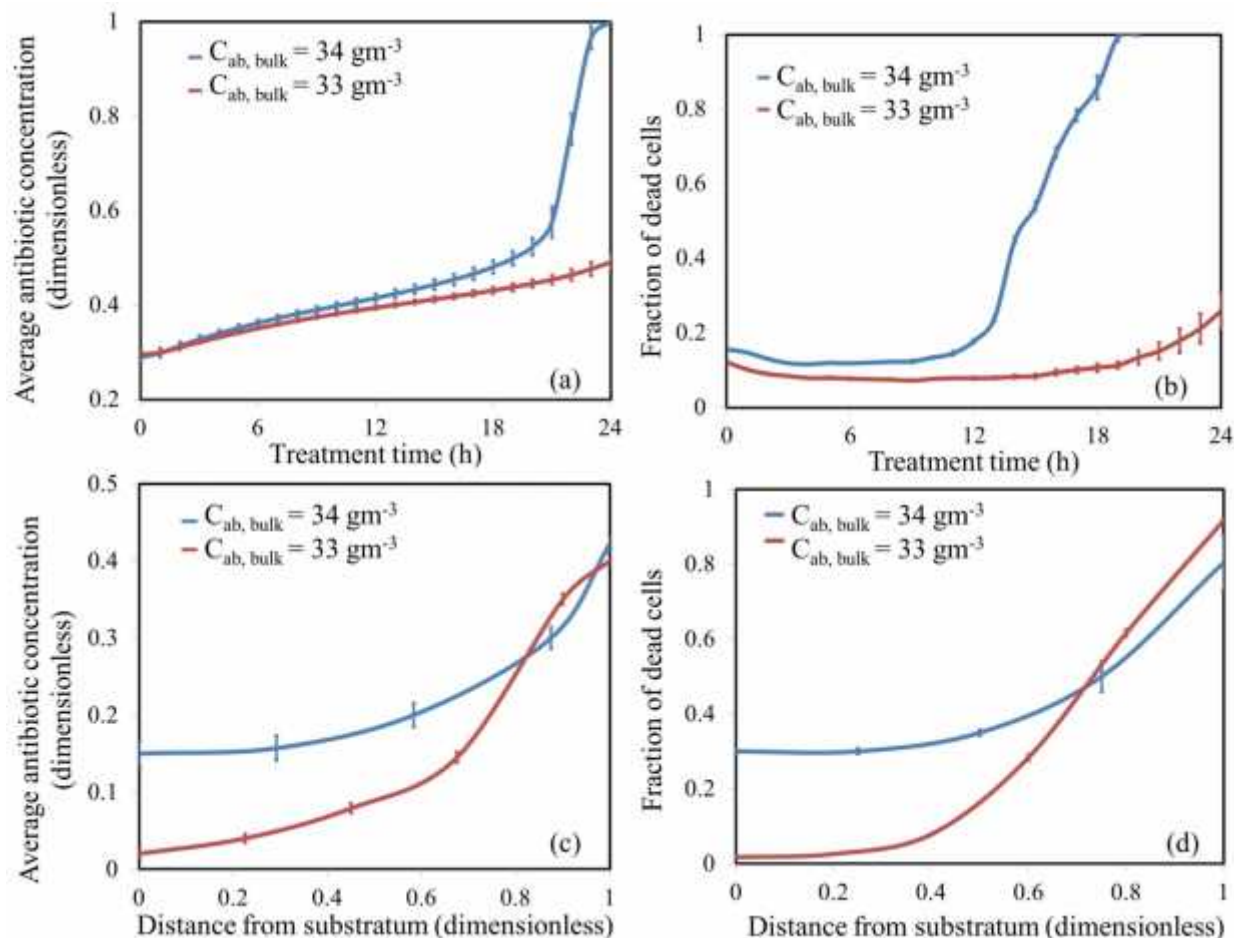
405 concentration (33 gm^{-3}) was insufficient to eradicate the biofilm. Interestingly, biofilms treated

406 with sub-MBEC ($C_{ab,bulk}$ of 33 gm^{-3}) exhibited a prolonged lifetime compared to even the

407 untreated biofilms, with the former sloughing off at 113 ± 0.5 h while the latter at 184 ± 2.7 h
408 (Fig. 1a). This is in line with the experimental observation that sub-MBEC treatment enhances
409 biofilm formation [59]. The average nutrient concentration within the sub-MBEC-treated
410 biofilm increased monotonically with time, and was higher compared to the untreated one (Fig.
411 1b). This is a consequence of the fact that antibiotic-induced cell death in the sub-MBEC-
412 treated biofilm causes the live cell number – and hence, the overall nutrient consumption – to
413 decrease. In contrast, bacterial biomass in the untreated biofilm increases with time, resulting in
414 increased nutrient consumption and reduced average nutrient concentration compared to the sub-
415 MBEC-treated biofilm. The spatial distribution of nutrient concentration (measured as a
416 function of the distance from the substratum) shows that nutrient penetration to the lower layers
417 in the untreated biofilm was lower compared to the treated biofilm (Fig. 1c). This, in turn,
418 causes cell death to occur near the bottom for the untreated biofilm, subsequently leading to
419 sloughing (Fig. 1d). These findings are in agreement with experimental results showing that
420 localized nutrient starvation is an environmental cue for the sloughing of biofilms [60]. In
421 contrast, cell death was restricted to the top layers in the sub-MBEC-treated biofilm (Fig.
422 1d). In agreement with experimental observations, sub-MBEC-treatment does not fully
423 eradicate bacteria during the treatment phase [61], and biofilm thickness was restored to pre-
424 treatment levels within 24 h after exposure to the antibiotic.

425
426 MBEC for the QS^+ biofilm was 51 gm^{-3} , and was significantly higher than that for QS^- .
427 Comparing responses of the QS^- and QS^+ biofilms when subjected to a bulk antibiotic
428 concentration of 34 gm^{-3} showed that whereas there was no significant difference in the viable
429 cell counts for the first 8 hours of treatment, the live cell number for the QS^+ biofilm reduced at
430 a lower rate for the rest of the treatment (Fig. 1a).

431
432



435
 436
 437 **Fig. 2. Response of the biofilm to MBEC and sub-MBEC treatments.** The average antibiotic
 438 concentration (a) and fraction of dead cells (b) as a function of time, upon treatment with MBEC
 439 (blue) and sub-MBEC (red). Spatial profiles for antibiotic concentration (c), and fraction of
 440 dead cells (d) after 16 h of treatment for the MBEC-treated (blue) and sub-MBEC-treated (red)
 441 biofilms. Data represent mean \pm standard error of mean (SEM) of four replicate simulations.
 442

443 To investigate the dramatically different responses of the QS^- biofilms subjected to two slightly
 444 different antibiotic concentrations (MBEC and sub-MBEC), we tracked the temporal variation
 445 in the average antibiotic concentrations within the biofilms. A small difference in the bulk
 446 antibiotic concentrations (1 gm^{-3}) was amplified to a much larger difference in average antibiotic
 447 concentrations within the biofilms; this difference was more pronounced at higher time points
 448 (after ~ 12 h of treatment) (Fig. 2a). This, in turn, led to higher cell death events in MBEC-
 449 treated biofilms compared to the ones treated with sub-MBEC (Fig. 2b). Under these conditions
 450 (after ~ 12 h of treatment), antibiotic penetration to the lower layers was more effective in the
 451 biofilm treated with MBEC compared to the one treated with sub-MBEC (Fig. 2c). For
 452 instance, after 16 h of treatment, the average antibiotic concentration at the substratum of the
 453 biofilm exposed to MBEC was ~ 7.5 times that of the biofilm treated with sub-MBEC (Fig.
 454 2c). This marked difference in local antibiotic concentrations in the lower regions of the biofilm

455 resulted in significantly higher death events for the MBEC-treated biofilm compared to the
456 biofilm treated with sub-MBEC (Fig. 2d). Whereas ~30% of the cells in the lowest layer died
457 when the biofilm was subjected to MBEC, negligible cell death (~2%) occurred near the
458 substratum of the sub-MBEC-treated biofilm (Fig. 2d). This difference in the fraction of dead
459 cells at the bottom layers of the biofilm was observed at all treatment time points, ultimately
460 leading to the eradication of the MBEC-treated biofilm. Similar trends were observed for the
461 QS+ biofilm upon MBEC- (51 gm^{-3}) and sub-MBEC (50 gm^{-3}) treatments (data not shown).

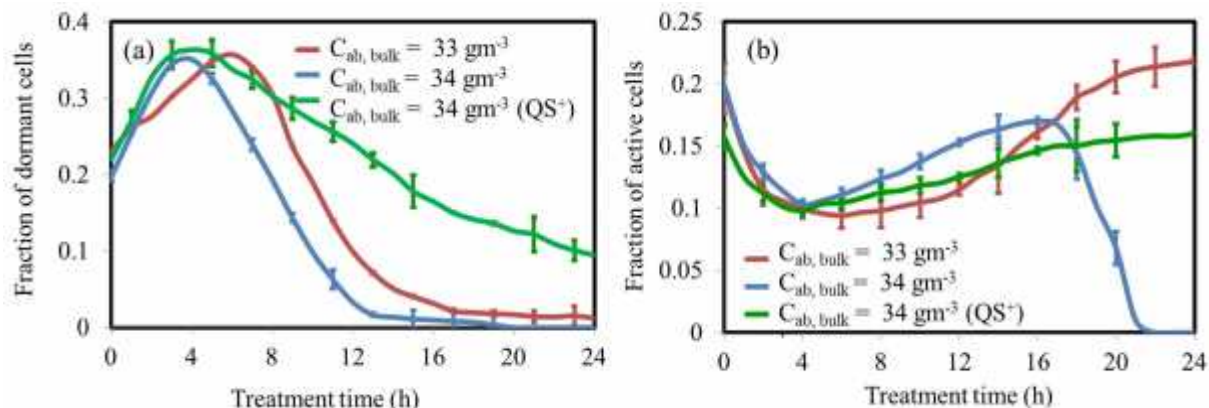
462

463 *Correlation between cellular metabolism rates and antibiotic-induced death*

464 Biofilms comprise of bacterial cells in a wide range of physiological states, resulting in a
465 spatially heterogeneous system. To investigate the influence of this spatial heterogeneity on the
466 response of the biofilm to MBEC- and sub-MBEC treatments, we categorized live cells into
467 three groups based on their growth rates: (i) metabolically active cells, exhibiting high growth
468 rates (HGR), (ii) intermediate, and (iii) dormant cells, exhibiting low growth rates
469 (LGR). There was a strong correlation between dead cells and HGR-cells in the presence of
470 antibiotic treatment. On an average, during treatment, $59.79 \pm 6.1\%$ of HGR died at any given
471 time step. On the other hand, LGR-cells were less susceptible to killing by antibiotic (~
472 0.001%). In stark contrast, in the absence of antibiotic treatment, there was a strong correlation
473 between dead cells and LGR-cells, with $34.15 \pm 2.8\%$ of LGR dying on an average at any given
474 time step. Under these conditions, cell death occurred predominantly due to nutrient starvation
475 at later time points (80 h onwards). The number of dead HGR-cells was negligible in the
476 untreated biofilm.

477

478



481
 482
 483 **Fig. 3. Growth dynamics of subpopulations in the presence of antibiotic.** Comparison of
 484 fraction of dormant cells (a), fraction of metabolically active cells (b) as a function of time for
 485 $C_{N,bulk} = 4 \text{ gm}^{-3}$. QS⁻ biofilms treated with MBEC (blue) and sub-MBEC (red), and QS⁺
 486 biofilm subjected to $C_{ab,bulk}$ of 34 gm^{-3} (green). Data represent mean \pm standard error of mean
 487 (SEM) of four replicate simulations.
 488

489 We tracked the dynamics of the distinct growth-rate-based cell subpopulations in QS⁻ and QS⁺
 490 biofilms in response to antibiotic treatment. Based on the fraction of HGR- and LGR-cells,
 491 three distinct phases were observed during 24 h of continuous antibiotic treatment (Figs. 3a and
 492 3b). In the first phase that lasted ~ 4 h, the total biomass reduced dramatically ($\sim 40\%$ reduction).
 493 In this phase, the fraction of dormant cells increased with time, reaching a peak after 4h of
 494 treatment (Fig. 3a). On the other hand, the subpopulation of active cells decreased with time
 495 (Fig. 3b). After 4 h, the antibiotic consumption rates by dormant cells in the MBEC-treated
 496 biofilms were ~ 17 times higher compared to those of active cells ($50.5 \pm 9.4 \text{ gm}^{-3} \text{ h}^{-1}$ for
 497 dormant cells, versus $850.5 \pm 65.4 \text{ gm}^{-3} \text{ h}^{-1}$ for active cells). This indicates that metabolically
 498 active cells at the distal edge of the biofilm act as a reaction-diffusion barrier, thereby reducing
 499 antibiotic penetration to the LGR-cells near the substratum. This results in lower antibiotic
 500 uptake rates by the LGR-cells, allowing them to survive antibiotic treatment. The second phase
 501 lasted for ~ 8 h, and was characterized by a decrease in the number of dormant cells (Fig. 3a).
 502 For the biofilm treated with MBEC, phases I and II were qualitatively similar to those observed
 503 for sub-MBEC treated biofilm. However phase II is delayed and prolonged in the biofilms
 504 treated with sub-MBEC (~ 5 h to 18 h) in comparison with MBEC-treated biofilms (4h to 12 h).
 505 The third phase was characterized by the complete eradication of the MBEC-treated biofilm. In
 506 contrast, the sub-MBEC-treated biofilm survived in phase III. More importantly, the fraction of
 507 active cells in the third phase of sub-MBEC treatment increased, resulting in the regrowth of the
 508 biofilm after the termination of antibiotic treatment.
 509

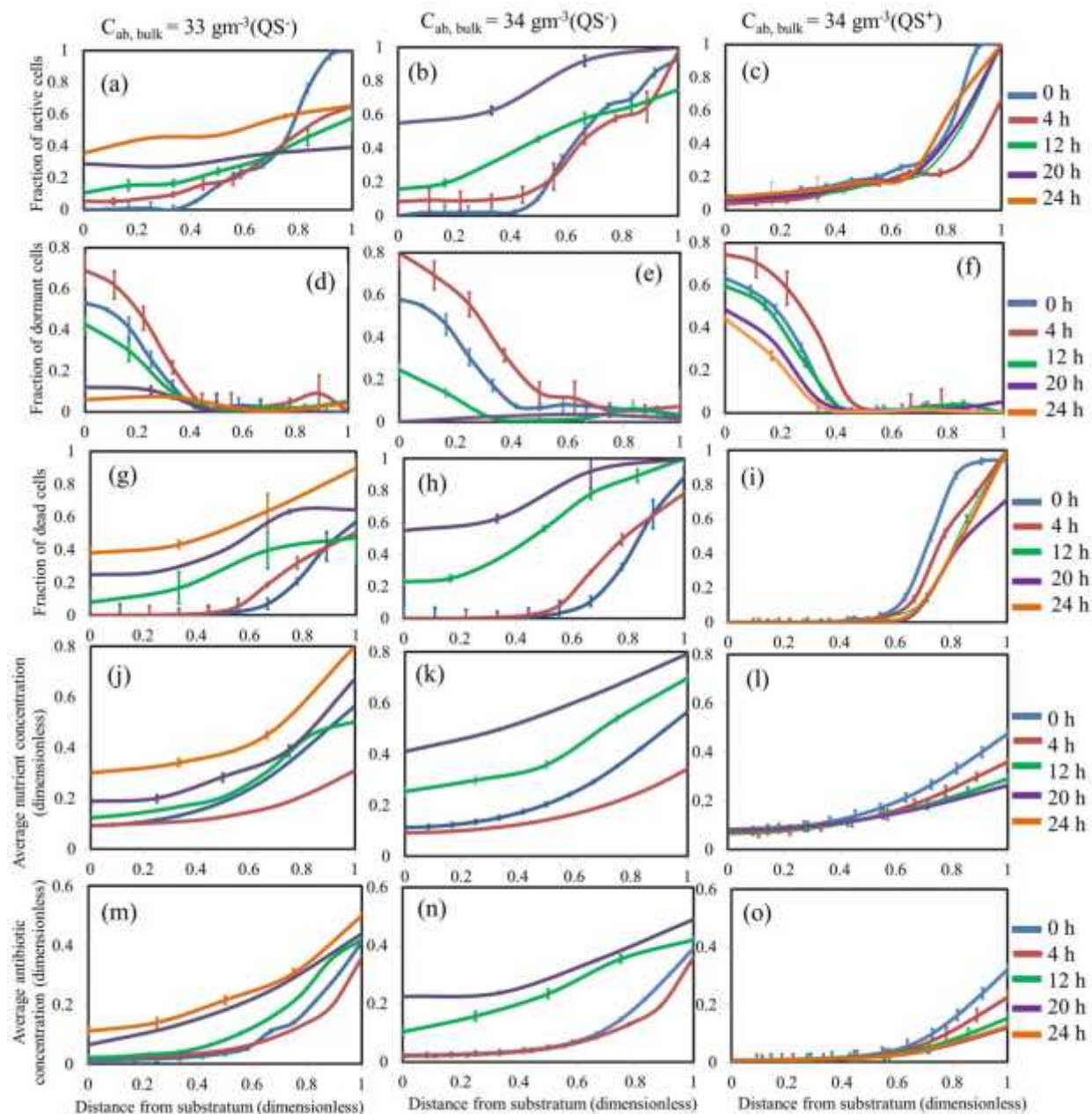
510 The QS⁺ biofilm survived treatment at $C_{ab,bulk}$ of 34 gm^{-3} . In contrast to the QS⁻ biofilm, the
 511 fraction of dormant cells increased monotonically in the third phase of QS⁺ biofilms (Fig. 3a).
 512 This could be a direct consequence of the increased viable cell number during treatment (Fig.
 513 1a), resulting in reduced nutrient availability in the lower regions of the biofilm. This starvation
 514 may lead to lower metabolic activity. Although both QS⁻ and QS⁺ biofilm survived treatment

515 with 33 gm^{-3} , the mechanisms of survival appear to be different. Whereas the QS^- biofilm
516 survives by rapidly transforming the metabolically inactive cells into active ones, the survival of
517 the QS^+ biofilm is a consequence of reduced exposure of the dormant cells to antibiotic.

518

519

520



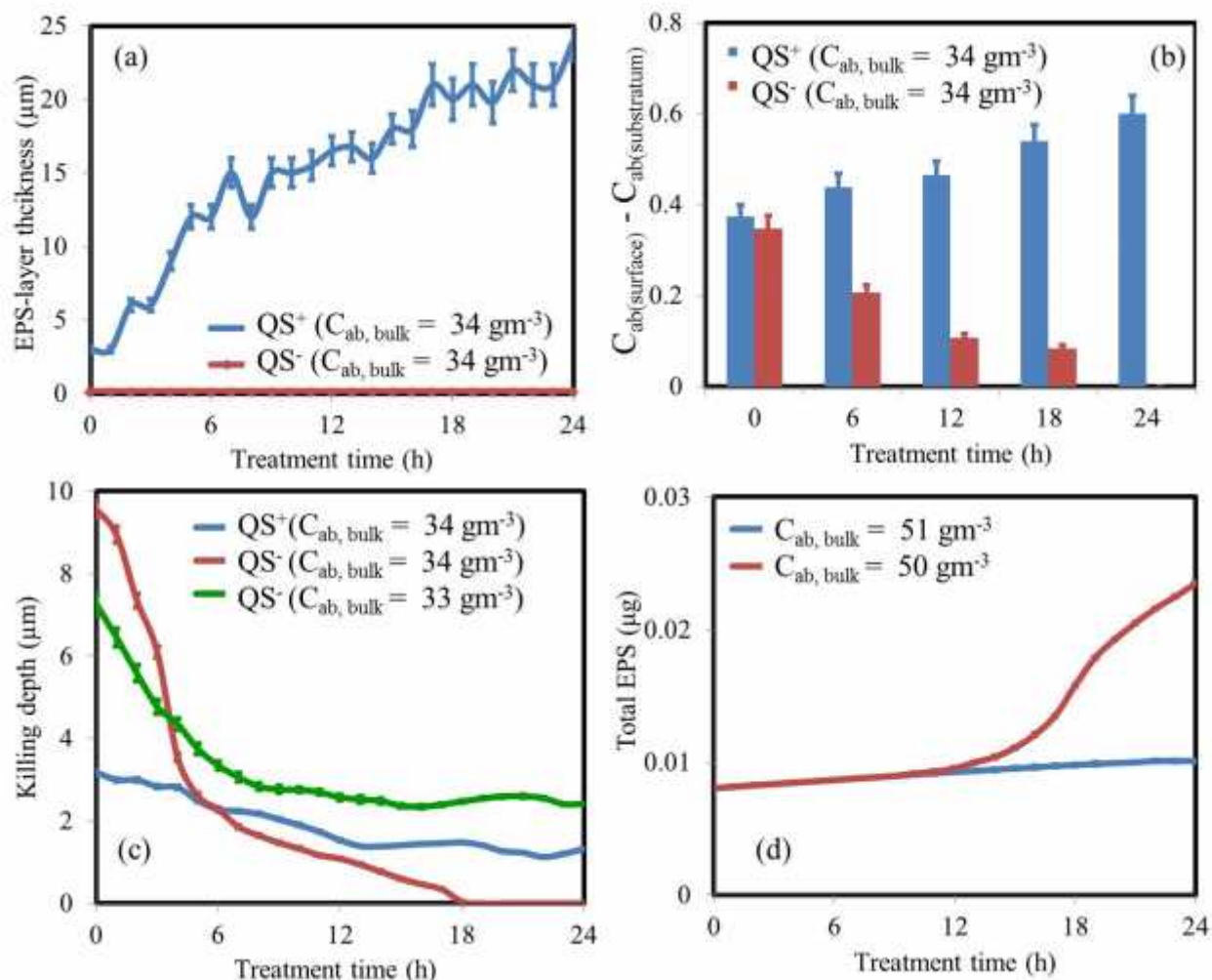
523
 524
 525 **Fig. 4. Spatial heterogeneity in treated QS⁻ and QS⁺ biofilm.** Comparison of sub-MBEC
 526 (panels a, d, g, j, and m) and MBEC-treated QS⁻ biofilms (panels b, e, h, k, n) and MBEC-
 527 treated QS⁺ biofilms (panels c, f, i, l, o) at different time points during 24 h treatment period.
 528 The spatial distribution of the fraction of dormant cells (panels a-c), active cells (panels d-f), and
 529 dead cells (panels g-i), local nutrient (panels j-l), and antibiotic concentrations (m-o). Data
 530 represent mean \pm standard error of mean (SEM) of four replicate simulations.

531
 532 To investigate the biophysical mechanisms for the formation of surviving cell pockets within the
 533 antibiotic-treated biofilm, we tracked the growth rates of individual cells, the distribution of

534 dead cells, and local nutrient and antibiotic concentrations as a function of their position within
535 the biofilm. Prior to exposure to antibiotics (64 h of growth), a majority of the metabolically
536 active cells are located at the upper layers (Figs. 4a-c), and dormant cells are localized at the
537 lower layers (Figs. 4d-f). Upon initiation of treatment, cells at the biofilm-bulk liquid interphase
538 are exposed to the antibiotic, resulting in cell death; cell death in the lower regions during this
539 time period is negligible (Figs. 4g-i). Because of the consumption of antibiotic by active cells in
540 the top layers, antibiotic penetration to lower layers is reduced (Figs. 4m-o). Cells in the lower
541 layers are, thus, able to survive the initial period of treatment. Consequently, the fraction of
542 dormant cells increases near the substratum and active cells decreased at the top (Figs. 4d-f). At
543 the end of phase I (4-6 h of treatment), nutrient penetration increased to the interior of the
544 biofilm (Figs. 4j, 4k). Subsequently, dormant cells located in the lower layers of the biofilm had
545 improved nutrient accessibility, resulting in increased growth rates. This, in turn, results in the
546 transformation of inactive cells to the metabolically active state. This is validated by the
547 observation that the fraction of dormant cells decreases and the fraction of active cells increases
548 near the substratum over time (Figs. 4a, 4b, 4d, 4e).

549
550 Antibiotic penetration to the lower layers in the MBEC-treated biofilm was higher compared to
551 that in the sub-MBEC-treated biofilm (Fig. 4m, 4n). In the surviving QS^+ biofilm (exposed to
552 $C_{ab,bulk}$ of 34 gm^{-3}), even the topmost bacterial cell was exposed to a local antibiotic
553 concentration that was always less than 30% of the bulk value (Fig. 4o). This is a direct
554 consequence of the sequestration of the antibiotic by the cell-devoid layer of EPS that forms at
555 the distal edge of the biofilm (Fig. 5a). In stark contrast, in the QS^- biofilm subjected to
556 treatment with MBEC, the local antibiotic concentration even at the substratum increased with
557 time, reaching a maximum value of 22.5% of the bulk antibiotic concentration (after 20 h of
558 treatment). Under these conditions, the local antibiotic concentration to which the topmost cell
559 in the biofilm was exposed was as high as 50%.

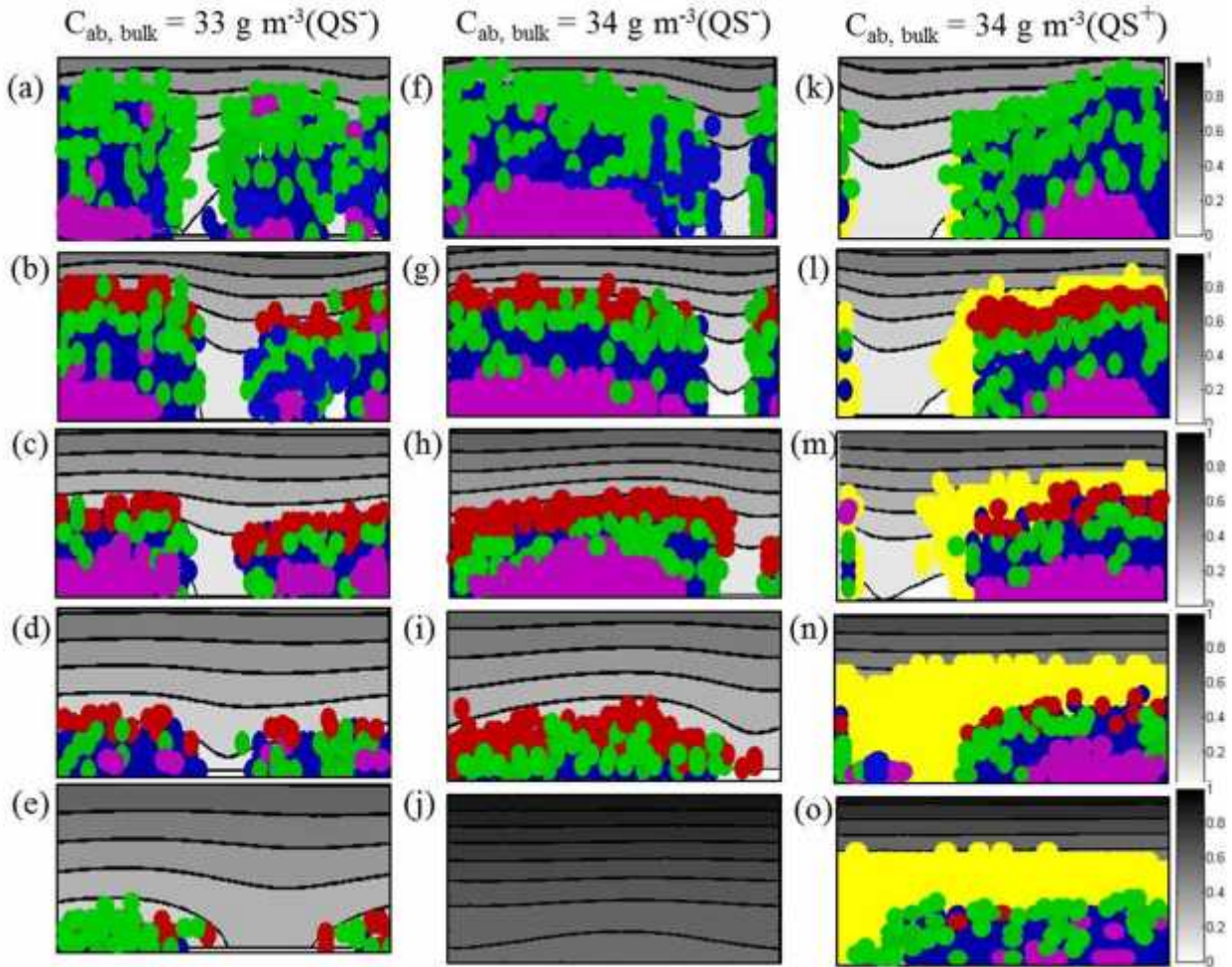
560
561



564
 565
 566 **Fig. 5. Comparison of the response of QS⁺ and QS⁻ biofilms to antibiotic treatment.**
 567 Thickness of the cell-devoid layer of EPS at the top of the biofilm plotted as a function of
 568 treatment time (a), the difference between the average antibiotic concentrations at the biofilm
 569 surface and the substratum for QS⁺ (blue) and QS⁻ (red) biofilms subjected to C_{ab,bulk} of 34 gm⁻³
 570 ³ (b), the average killing depth for QS⁺ (blue) and QS⁻ biofilms subjected to C_{ab,bulk} of 34 gm⁻³
 571 (red) and C_{ab,bulk} of 33 gm⁻³ (green) (c), and the total EPS produced for QS⁺ biofilms subjected
 572 to C_{ab,bulk} of 50 gm⁻³ (red) and C_{ab,bulk} of 51 gm⁻³ (blue) (d). Data represent mean ± standard
 573 error of mean (SEM) of four replicate simulations.

574
 575 Next, we compared the responses of the QS⁻ (MBEC = 33 gm⁻³) and QS⁺ (MBEC = 51 gm⁻³)
 576 biofilms subjected to C_{ab,bulk} of 34 gm⁻³. A cell-devoid layer of EPS is formed at the top of the
 577 QS⁺ biofilm, and the thickness of this layer increases as treatment proceeds (Fig. 5a). The
 578 extent of antibiotic penetration was quantified as the difference between the average antibiotic
 579 concentration at the surface of the biofilm and that at the substratum; lower the difference,

580 higher the extent of penetration. Antibiotic penetration in the QS⁺ biofilm was significantly
581 lower compared to that in the QS⁻ biofilm (Fig. 5b), indicating that EPS sequesters antibiotic,
582 thereby lowering the local concentrations in the interior of the biofilm. The largest distance
583 from the surface of the biofilm at which antibiotic-induced cell death occurs was termed the
584 killing depth. In agreement with the observation of fig. 5b, the killing depth for the QS⁻ biofilms
585 was higher than that for the QS⁺ biofilm. The killing depth decreased monotonically with time
586 for both QS⁻ and QS⁺ biofilms as the biofilm thickness reduced. Interestingly, the QS⁺ biofilm
587 subjected to a sub-MBEC treatment (C_{abbulk} of 51 gm⁻³) exhibited enhanced EPS production
588 compared to that when subjected to the MBEC treatment (Fig. 5d).
589



590

591

592

593 **Fig. 6. QS⁻ Biofilms treated with sub-MBEC (a, b, c, d, e) and MBEC (f, g, h, i, j), and QS⁺**
 594 **biofilms treated with MBEC (k, l, m, n, o).** Visualization of 2D cross-sections showing high
 595 growth rate (green), intermediate growth rate cells (cyan), low-growth rate (blue), and locations
 596 of cell death (red), of the $C_{N,bulk} = 4 \text{ gm}^{-3}$ biofilm after 0 h, 1 h, 4 h, 20 h, and 24 h of antibiotic
 597 introduction. The yellow color represents EPS in QS⁺ biofilm. The isolines show the antibiotic
 598 concentration distribution.

599

600 Fig. 6 shows representative biofilm cross-sections at various stages of the response, illustrating
 601 the formation of surviving cell pockets within antibiotic-treated QS⁻ and QS⁺ biofilms. After the
 602 first hour of treatment (panels 6a, 6e, and 6i), dormant cells (pink) were localized in the interior
 603 of the biofilm, and were surrounded by layers of cells exhibiting high (green), and intermediate
 604 (blue) growth rates. Antibiotic-induced cell death events (red) occurred at and near the biofilm-
 605 bulk liquid interface. For the QS⁻ biofilms, thickness reduces as treatment continues, resulting
 606 in increased nutrient availability in the bottom layers. This causes the slow-growing (pink) cells
 607 to transform into cells with intermediate- (blue) and high- (green) growth rates. This is evident
 608 by the diminishing population of slow-growing cells in panels (6b), (6c), (6g), and (6h). For the

609 QS⁺ biofilm, antibiotic-induced cell death events at the top resulted in the formation of a thin
610 cell-devoid layer of EPS (yellow). This result is in agreement with experimental investigations
611 that indicate that EPS was most abundant at the upper layers of the biofilm [62]. Antibiotic
612 penetration was hindered by an interaction with the matrix of EPS, and results in the protection
613 of bacterial cells in the lower layers. These results are in agreement with previous experimental
614 investigation that suggests that the production of EPS by QS, and the subsequent accumulation
615 in the upper regions of the biofilm, plays a key role in biofilm resistance [41].
616

617 **Conclusions**

618 Although bacteria are traditionally investigated as planktonic entities, they predominantly occur
619 as sessile, substratum-associated biofilms. Bacteria associated with the biofilm mode of growth
620 are more resistant to antibiotics, compared to their planktonic counterparts. Several hypotheses
621 have been proposed to explain this resistance including upregulation of virulence factors,
622 formation of persister cells, genetic manipulations, slow penetration of the antibiotic, and the
623 presence of dormant, slow-growing cells. Most of these mechanisms involve antibiotic
624 resistance at the single-cell level, and do not account for the effects of intercellular population
625 dynamics. Physical mechanisms of resistance like retarded penetration of the antibiotic may be
626 a factor in the early stages of treatment, but as treatment proceeds and cells at the top die,
627 antibiotic penetration to the lower layers increases. Hence, retarded penetration of the antibiotic
628 may not be a sufficient explanation as a protecting mechanism in biofilms.
629

630 Biofilms comprise of physiologically distinct subpopulations of cells exhibiting varying growth
631 rates, due in part to their adaptation to local environmental conditions. We have previously
632 characterized this spatial heterogeneity in biofilms [43]. Interestingly, response of biofilms to
633 an antibiotic challenge is also heterogeneous, with only certain subpopulations becoming
634 resistant while the rest of the biofilm remains sensitive. Our goal was to investigate the
635 influence of the biophysical features of the biofilm mode of growth on antibiotic resistance,
636 when each individual cell itself is not necessarily tolerant to antibiotics. This may help delineate
637 the effect of population dynamics on the antibiotic resistance in biofilms. We also wished to
638 correlate the inherent spatial heterogeneity of biofilms at the cellular level to their heterogeneous
639 response to treatment. Consequently, in our model, each bacterium was modeled as an
640 independent entity, allowing us to monitor structural and chemical heterogeneities in the biofilm
641 and in its response to treatment as a function of time and space.
642

643 We first estimated the minimum antibiotic concentration required to eradicate biofilms in our
644 simulations. This allowed us to identify the largest antibiotic concentration that the biofilm is
645 able to survive. These are the conditions we used to further investigate mechanisms of
646 antibiotic resistance in biofilms. Small differences in the bulk antibiotic concentrations were
647 amplified into much larger differences in local antibiotic concentrations to which cells are
648 exposed. When subjected to MBEC and sub-MBEC treatments, the local antibiotic
649 concentration near the substratum for the MBEC-treated biofilm was ~13 times higher compared
650 to that for the sub-MBEC-treated biofilm, although the difference in the bulk antibiotic
651 concentrations was small (1 gm⁻³). QS⁻ (non-EPS producing) biofilms, subjected to an antibiotic
652 challenge, responded by increasing the rate of transformation of dormant cells into faster
653 growing, metabolically active cells. In contrast, QS⁺ biofilms responded by enhancing the rate

654 of EPS production. Overall, insights into these biophysical mechanisms associated with the
655 biofilm mode of growth may pave the way for novel therapeutic strategies to combat the
656 antibiotic resistance of biofilms.

657

658 **Acknowledgments**

659 This work was supported by the Start-Up Research Grant (No. SB/YS/LS-210/2013), Science
660 and Engineering Research Board, India.

661

662 **References**

- 663 1. Donlan, R.M., *Biofilms: microbial life on surfaces*. Emerg Infect Dis, 2002. **8**(9): p. 881-90.
664 10.3201/eid0809.020063
- 665 2. Flemming, H.C., et al., *Biofilms: an emergent form of bacterial life*. Nat Rev Microbiol, 2016.
666 **14**(9): p. 563-75. 10.1038/nrmicro.2016.94
- 667 3. Leid, J.G., *Bacterial Biofilms Resist Key Host Defenses*. Microbe 2009. **4**(Number 2,): p. 66-70.
- 668 4. Hathroubi, S., et al., *Biofilms: Microbial Shelters Against Antibiotics*. Microb Drug Resist, 2017.
669 **23**(2): p. 147-156. 10.1089/mdr.2016.0087
- 670 5. Hall, C.W. and T.F. Mah, *Molecular mechanisms of biofilm-based antibiotic resistance and*
671 *tolerance in pathogenic bacteria*. FEMS Microbiol Rev, 2017. **41**(3): p. 276-301.
672 10.1093/femsre/fux010
- 673 6. Gupta, K., et al., *Antimicrobial tolerance of Pseudomonas aeruginosa biofilms is activated during*
674 *an early developmental stage and requires the two-component hybrid SagS*. J Bacteriol, 2013.
675 **195**(21): p. 4975-87. 10.1128/JB.00732-13
- 676 7. He, X. and J. Ahn, *Differential gene expression in planktonic and biofilm cells of multiple*
677 *antibiotic-resistant Salmonella Typhimurium and Staphylococcus aureus*. FEMS Microbiol Lett,
678 2011. **325**(2): p. 180-8. 10.1111/j.1574-6968.2011.02429.x
- 679 8. Wood, T.K., S.J. Knabel, and B.W. Kwan, *Bacterial persister cell formation and dormancy*. Appl
680 Environ Microbiol, 2013. **79**(23): p. 7116-21. 10.1128/AEM.02636-13
- 681 9. Pamp, S.J., et al., *Tolerance to the antimicrobial peptide colistin in Pseudomonas aeruginosa*
682 *biofilms is linked to metabolically active cells, and depends on the pmr and mexAB-oprM genes*.
683 Mol Microbiol, 2008. **68**(1): p. 223-40. 10.1111/j.1365-2958.2008.06152.x
- 684 10. Beaudoin, T., et al., *The biofilm-specific antibiotic resistance gene ndvB is important for*
685 *expression of ethanol oxidation genes in Pseudomonas aeruginosa biofilms*. J Bacteriol, 2012.
686 **194**(12): p. 3128-36. 10.1128/JB.06178-11
- 687 11. Lewis, K., *Multidrug tolerance of biofilms and persister cells*. Curr Top Microbiol Immunol, 2008.
688 **322**: p. 107-31.
- 689 12. LaFleur, M.D., C.A. Kumamoto, and K. Lewis, *Candida albicans biofilms produce antifungal-*
690 *tolerant persister cells*. Antimicrob Agents Chemother, 2006. **50**(11): p. 3839-46.
691 10.1128/AAC.00684-06
- 692 13. Sultana, S.T., D.R. Call, and H. Beyenal, *Eradication of Pseudomonas aeruginosa biofilms and*
693 *persister cells using an electrochemical scaffold and enhanced antibiotic susceptibility*. npj
694 Biofilms and Microbiomes, 2016. **2**(1): p. 2. 10.1038/s41522-016-0003-0
- 695 14. Gilbert, P., et al., *The physiology and collective recalcitrance of microbial biofilm communities*.
696 Adv Microb Physiol, 2002. **46**: p. 202-56.

- 697 15. Kostakioti, M., M. Hadjifrangiskou, and S.J. Hultgren, *Bacterial biofilms: development, dispersal,*
698 *and therapeutic strategies in the dawn of the postantibiotic era.* Cold Spring Harb Perspect Med,
699 2013. **3**(4): p. a010306. 10.1101/cshperspect.a010306
- 700 16. Stewart, P.S. and J.W. Costerton, *Antibiotic resistance of bacteria in biofilms.* Lancet, 2001.
701 **358**(9276): p. 135-8.
- 702 17. Stewart, P.S. and M.J. Franklin, *Physiological heterogeneity in biofilms.* Nat Rev Microbiol, 2008.
703 **6**(3): p. 199-210. 10.1038/nrmicro1838
- 704 18. Mah, T.F. and G.A. O'Toole, *Mechanisms of biofilm resistance to antimicrobial agents.* Trends
705 Microbiol, 2001. **9**(1): p. 34-9.
- 706 19. de la Fuente-Nunez, C., et al., *Bacterial biofilm development as a multicellular adaptation:*
707 *antibiotic resistance and new therapeutic strategies.* Curr Opin Microbiol, 2013. **16**(5): p. 580-9.
708 10.1016/j.mib.2013.06.013
- 709 20. Yang, L., et al., *In situ growth rates and biofilm development of Pseudomonas aeruginosa*
710 *populations in chronic lung infections.* J Bacteriol, 2008. **190**(8): p. 2767-76. 10.1128/JB.01581-
711 07
- 712 21. Williamson, K.S., et al., *Heterogeneity in Pseudomonas aeruginosa biofilms includes expression*
713 *of ribosome hibernation factors in the antibiotic-tolerant subpopulation and hypoxia-induced*
714 *stress response in the metabolically active population.* J Bacteriol, 2012. **194**(8): p. 2062-73.
715 10.1128/JB.00022-12
- 716 22. Haagensen, J.A., et al., *Differentiation and distribution of colistin- and sodium dodecyl sulfate-*
717 *tolerant cells in Pseudomonas aeruginosa biofilms.* J Bacteriol, 2007. **189**(1): p. 28-37.
718 10.1128/JB.00720-06
- 719 23. Walters, M.C., 3rd, et al., *Contributions of antibiotic penetration, oxygen limitation, and low*
720 *metabolic activity to tolerance of Pseudomonas aeruginosa biofilms to ciprofloxacin and*
721 *tobramycin.* Antimicrob Agents Chemother, 2003. **47**(1): p. 317-23.
- 722 24. Kolpen, M., et al., *Increased bactericidal activity of colistin on Pseudomonas aeruginosa biofilms*
723 *in anaerobic conditions.* Pathog Dis, 2016. **74**(1): p. ftv086. 10.1093/femspd/ftv086
- 724 25. Borriello, G., et al., *Oxygen limitation contributes to antibiotic tolerance of Pseudomonas*
725 *aeruginosa in biofilms.* Antimicrob Agents Chemother, 2004. **48**(7): p. 2659-64.
726 10.1128/AAC.48.7.2659-2664.2004
- 727 26. Mulcahy, L.R., V.M. Isabella, and K. Lewis, *Pseudomonas aeruginosa biofilms in disease.* Microb
728 Ecol, 2014. **68**(1): p. 1-12. 10.1007/s00248-013-0297-x
- 729 27. Ceri, H., et al., *The Calgary Biofilm Device: new technology for rapid determination of antibiotic*
730 *susceptibilities of bacterial biofilms.* J Clin Microbiol, 1999. **37**(6): p. 1771-6.
- 731 28. Hoffman, L.R., et al., *Aminoglycoside antibiotics induce bacterial biofilm formation.* Nature,
732 2005. **436**(7054): p. 1171-5. 10.1038/nature03912
- 733 29. Kiran, S., et al., *Enzymatic quorum quenching increases antibiotic susceptibility of multidrug*
734 *resistant Pseudomonas aeruginosa.* Iran J Microbiol, 2011. **3**(1): p. 1-12.
- 735 30. Kaplan, J.B., *Antibiotic-induced biofilm formation.* Int J Artif Organs, 2011. **34**(9): p. 737-51.
736 10.5301/ijao.5000027
- 737 31. Sailer, F.C., B.M. Meberg, and K.D. Young, *beta-Lactam induction of colanic acid gene expression*
738 *in Escherichia coli.* FEMS Microbiol Lett, 2003. **226**(2): p. 245-9.
- 739 32. Atkinson, S. and P. Williams, *Quorum sensing and social networking in the microbial world.* J R
740 Soc Interface, 2009. **6**(40): p. 959-78. 10.1098/rsif.2009.0203
- 741 33. de Kievit, T.R. and B.H. Iglewski, *Bacterial quorum sensing in pathogenic relationships.* Infect
742 Immun, 2000. **68**(9): p. 4839-49.
- 743 34. Ng, W.L. and B.L. Bassler, *Bacterial quorum-sensing network architectures.* Annu Rev Genet,
744 2009. **43**: p. 197-222. 10.1146/annurev-genet-102108-134304

- 745 35. Sakuragi, Y. and R. Kolter, *Quorum-sensing regulation of the biofilm matrix genes (pel) of*
746 *Pseudomonas aeruginosa*. J Bacteriol, 2007. **189**(14): p. 5383-6. 10.1128/JB.00137-07
- 747 36. Quinones, B., G. Dulla, and S.E. Lindow, *Quorum sensing regulates exopolysaccharide*
748 *production, motility, and virulence in Pseudomonas syringae*. Mol Plant Microbe Interact, 2005.
749 **18**(7): p. 682-93. 10.1094/MPMI-18-0682
- 750 37. von Bodman, S.B., D.R. Majerczak, and D.L. Coplin, *A negative regulator mediates quorum-*
751 *sensing control of exopolysaccharide production in Pantoea stewartii subsp. stewartii*. Proc Natl
752 Acad Sci U S A, 1998. **95**(13): p. 7687-92.
- 753 38. Davies, D.G., et al., *The involvement of cell-to-cell signals in the development of a bacterial*
754 *biofilm*. Science, 1998. **280**(5361): p. 295-8.
- 755 39. Tseng, B.S., et al., *The extracellular matrix protects Pseudomonas aeruginosa biofilms by limiting*
756 *the penetration of tobramycin*. Environ Microbiol, 2013. **15**(10): p. 2865-78. 10.1111/1462-
757 2920.12155
- 758 40. Shih, P.C. and C.T. Huang, *Effects of quorum-sensing deficiency on Pseudomonas aeruginosa*
759 *biofilm formation and antibiotic resistance*. J Antimicrob Chemother, 2002. **49**(2): p. 309-14.
- 760 41. Davenport, E.K., D.R. Call, and H. Beyenal, *Differential protection from tobramycin by*
761 *extracellular polymeric substances from Acinetobacter baumannii and Staphylococcus aureus*
762 *biofilms*. Antimicrob Agents Chemother, 2014. **58**(8): p. 4755-61. 10.1128/AAC.03071-14
- 763 42. Brackman, G., et al., *The Quorum Sensing Inhibitor Hamamelitannin Increases Antibiotic*
764 *Susceptibility of Staphylococcus aureus Biofilms by Affecting Peptidoglycan Biosynthesis and*
765 *eDNA Release*. Sci Rep, 2016. **6**: p. 20321. 10.1038/srep20321
- 766 43. Machineni, L., et al., *Influence of Nutrient Availability and Quorum Sensing on the Formation of*
767 *Metabolically Inactive Microcolonies Within Structurally Heterogeneous Bacterial Biofilms: An*
768 *Individual-Based 3D Cellular Automata Model*. Bull Math Biol, 2017. **79**(3): p. 594-618.
769 10.1007/s11538-017-0246-9
- 770 44. Fagerlind, M.G., et al., *Dynamic modelling of cell death during biofilm development*. J Theor Biol,
771 2012. **295**: p. 23-36. 10.1016/j.jtbi.2011.10.007
- 772 45. Picioreanu, C., J.U. Kreft, and M.C. Van Loosdrecht, *Particle-based multidimensional multispecies*
773 *biofilm model*. Appl Environ Microbiol, 2004. **70**(5): p. 3024-40.
- 774 46. Eberl H, M.E., Noguera D, Picioreanu C, Rittmann B, van Loosdrecht M, Wanner O *Mathematical*
775 *modeling of biofilms*. IWA Publishing, 2006.
- 776 47. Castro, S.L., et al., *Induction of attachment-independent biofilm formation and repression of Hfq*
777 *expression by low-fluid-shear culture of Staphylococcus aureus*. Appl Environ Microbiol, 2011.
778 **77**(18): p. 6368-78. 10.1128/AEM.00175-11
- 779 48. Guo, P., A.M. Weinstein, and S. Weinbaum, *A hydrodynamic mechanosensory hypothesis for*
780 *brush border microvilli*. Am J Physiol Renal Physiol, 2000. **279**(4): p. F698-712.
- 781 49. Picioreanu, C., M.C. Van Loosdrecht, and J.J. Heijnen, *Effect of diffusive and convective substrate*
782 *transport on biofilm structure formation: a two-dimensional modeling study*. Biotechnol Bioeng,
783 2000. **69**(5): p. 504-15.
- 784 50. Falsetta, M.L., et al., *Symbiotic relationship between Streptococcus mutans and Candida albicans*
785 *synergizes virulence of plaque biofilms in vivo*. Infect Immun, 2014. **82**(5): p. 1968-81.
786 10.1128/IAI.00087-14
- 787 51. Pizarro, G.E., et al., *Two-dimensional cellular automaton model for mixed-culture biofilm*. Water
788 Sci Technol, 2004. **49**(11-12): p. 193-8.
- 789 52. Fozard, J.A., et al., *Inhibition of quorum sensing in a computational biofilm simulation*.
790 Biosystems, 2012. **109**(2): p. 105-14. 10.1016/j.biosystems.2012.02.002
- 791 53. Frederick, M.R., et al., *A mathematical model of quorum sensing regulated EPS production in*
792 *biofilm communities*. Theor Biol Med Model, 2011. **8**: p. 8. 10.1186/1742-4682-8-8

- 793 54. Chambless, J.D., S.M. Hunt, and P.S. Stewart, *A three-dimensional computer model of four*
794 *hypothetical mechanisms protecting biofilms from antimicrobials*. Appl Environ Microbiol, 2006.
795 **72**(3): p. 2005-13. 10.1128/AEM.72.3.2005-2013.2006
- 796 55. Schaule, G., H.C. Flemming, and H.F. Ridgway, *Use of 5-cyano-2,3-ditolyl tetrazolium chloride for*
797 *quantifying planktonic and sessile respiring bacteria in drinking water*. Appl Environ Microbiol,
798 1993. **59**(11): p. 3850-7.
- 799 56. Manuel, C.M., O.C. Nunes, and L.F. Melo, *Dynamics of drinking water biofilm in flow/non-flow*
800 *conditions*. Water Res, 2007. **41**(3): p. 551-62. 10.1016/j.watres.2006.11.007
- 801 57. Leisner, M., et al., *Kinetics of genetic switching into the state of bacterial competence*. Biophys J,
802 2009. **96**(3): p. 1178-88. 10.1016/j.bpj.2008.10.034
- 803 58. Ardre, M., et al., *An individual-based model for biofilm formation at liquid surfaces*. Phys Biol,
804 2015. **12**(6): p. 066015. 10.1088/1478-3975/12/6/066015
- 805 59. Cerca, N., et al., *Effects of growth in the presence of subinhibitory concentrations of dicloxacillin*
806 *on Staphylococcus epidermidis and Staphylococcus haemolyticus biofilms*. Appl Environ
807 Microbiol, 2005. **71**(12): p. 8677-82. 10.1128/AEM.71.12.8677-8682.2005
- 808 60. Hunt, S.M., et al., *Hypothesis for the role of nutrient starvation in biofilm detachment*. Appl
809 Environ Microbiol, 2004. **70**(12): p. 7418-25. 10.1128/AEM.70.12.7418-7425.2004
- 810 61. Shen, Y., et al., *Experimental and Theoretical Investigation of Multispecies Oral Biofilm*
811 *Resistance to Chlorhexidine Treatment*. Sci Rep, 2016. **6**: p. 27537. 10.1038/srep27537
- 812 62. Roldan, M.H.-M.a.M., *Characterization of Photosynthetic Biofilms from Roman Catacombs via*
813 *3D Imaging and Subcellular Identification of Pigments*. COALITION, 2007(15).
- 814 63. Koerber, A.J., et al., *A mathematical model of partial-thickness burn-wound infection by*
815 *Pseudomonas aeruginosa: quorum sensing and the build-up to invasion*. Bull Math Biol, 2002.
816 **64**(2): p. 239-59. 10.1006/bulm.2001.0272
- 817 64. Moskowitz, S.M., et al., *Clinically feasible biofilm susceptibility assay for isolates of Pseudomonas*
818 *aeruginosa from patients with cystic fibrosis*. J Clin Microbiol, 2004. **42**(5): p. 1915-22.

819

820

821

822 Table I. Model parameters

Parameter	Description	Value	Unit	Reference
Δx	Element length	3	μm	
δ	Thickness of the DBL	18	μm	[43]
N_x	Number of elements in the x direction	40		
N_0	Initial number of bacterial cells	6		
m_0	Maintenance coefficient	0.036	h^{-1}	[43]
μ_{max}	Maximum specific growth rate of bacterial population	0.3125	h^{-1}	[43]
Y_{NB}	Yield coefficient for biomass	0.45		[43]
t_{SP}	Time in the stationary phase at which cell death occurs	24	h	[43]
r_{min}	Ratio of the rate of nutrient consumption to that of endogenous metabolism below which cell death occurs	0.15		[43]
B_{thr}	Threshold biomass at which cell division occurs	2×10^{-12}	g	
D_N	Diffusion coefficient of nutrient	0.84×10^{-6}	$\text{m}^2 \text{s}^{-1}$	[43]
K_N	Monod saturation constant	2.55	g m^{-3}	[43]
$C_{N,bulk}$	Bulk nutrient concentration	4	g m^{-3}	
Y_{EN}	Yield coefficient for EPS	0.27		[43]
$C_{EPS,thr}$	Threshold concentration at which EPS division occurs	33000	g m^{-3}	[43]
D_A	Diffusion coefficient of autoinducer	1×10^{-6}	$\text{m}^2 \text{s}^{-1}$	
r_{Au}	Autoinducer production rate by up-regulated cells	73800	$\text{m}^3 \text{h}^{-1}$ molecules h^{-1} [52]	[52]
r_{Ad}	Autoinducer production rate by down-regulated cells	498	molecules h^{-1} [52] molecules h^{-1} [52]	[52]
α	Spontaneous up-regulation rate	7.89×10^{-17}	molecules h^{-1} [52] $\text{m}^3 \text{molecule}^{-1} \text{h}^{-1}$ [52, 63]	[52, 63]
β	Spontaneous down-regulation rate	0.975	h^{-1}	[52, 63]

γ	Transition constant	7.96×10^{-17}	$\text{m}^{-3} \cdot \text{mole}^{-1} \cdot \text{s}^{-1}$ [52, 63]	[52, 63]
D_{ab}	Diffusion coefficient of antibiotic	0.36×10^{-6}	$\text{m}^2 \cdot \text{s}^{-1}$	[54]
$\frac{D_{ab}}{K_{ab}}$	Antibiotic half-saturation coefficient	1	$\text{m}^2 \cdot \text{s}^{-1} \cdot \text{m}^{-3}$	[54]
$\frac{h_{ab}}{K_{ab}^{max}}$	Maximum specific reaction rate of antibiotic with bacterial cell	2.5	h^{-1}	[54]
BIC	Biofilm inhibitory concentration	1- 64	m^{-3}	[64]
$\frac{h_{ab}}{K_{ab}^{max}}$	Maximum specific reaction rate of antibiotic with EPS	0.25	h^{-1}	